Computer-Aided Design 152 (2022) 103394

Contents lists available at ScienceDirect

Computer-Aided Design

journal homepage: www.elsevier.com/locate/cad

Geometry-based Assurance of Directional Solidification for Complex Topology-optimized Castings using the Medial Axis Transform

Maximilian Erber [a,1,*], Tobias Rosnitschek [b,1], Christoph Hartmann [a], Bettina Alber-Laukant [b], Stephan Tremmel [b], Wolfram Volk [a]

[a] Metal Forming and Casting, Technical University Munich, Walther-Meissner-Strasse 4, 85748 Garching, Germany
[b] Engineering Design and CAD, University of Bayreuth, Universitaetsstr. 30, 95447 Bayreuth, Germany

ARTICLE INFO

Article history:
Received 23 December 2021
Received in revised form 8 July 2022
Accepted 2 August 2022

Keywords:
Medial axis
Topology optimization
Solidification
Geometrical approach
Casting design

ABSTRACT

Using structural optimization is ideal for the development of complex aluminum cast parts, due to the high degree of design freedom. Various casting processes exist for production, and these differ in their boundary conditions and process restrictions. The resulting geometric restrictions have so far only been taken into account to a limited extent in structural optimization. Hence, there is a desire to determine simple process restrictions that can be taken into account to generate component geometries that are as light as possible but can still be produced by casting. This paper addresses the automated validation and optimization of directional solidification for topology-optimized geometries for castings. For the parametric description of the component volume, the medial axis transform (MAT) method is chosen. This approach allows a subsequent evaluation and optimization by methods of graph theory and feedback into an adapted surface file. The optimization results are finally evaluated by a process simulation using the finite volume method.

1. Introduction

Lightweight structures and load-adapted components continue to play a prominent role in discussions on climate neutrality and energy efficiency. Due to the wide range of possible components with complex structures and high functional integration combined with efficient production, casting processes are among the most frequently used manufacturing methods for such optimized components. Aluminum alloys are in particular used for this purpose because of the high lightweight potential of the material.

To minimize product development times and meet the increasing demands on cast aluminum components, use of topology optimization and casting simulations has become standard. However, up until now, topology optimization, i.e. the load-adapted design of the component, and casting simulation, i.e. the manufacturing-appropriate design of the component, have been insufficiently coupled.

In this paper, we introduce an approach for coupling the load-adapted and the manufacturing-appropriate design. To ensure compliance with the manufacturing constraints during the topology optimization, we use a geometry-based substitute model that estimates directional solidification purely on the basis of the component shape using the medial axis transform.

2. Background

Casting processes allow the near-net-shape fabrication of thin-walled lightweight components [1]. In doing so, liquid metal fills a mold replacing the air that previously filled it. After filling, the metal solidifies in the desired geometry of the cavity. During solidification the specific volume of the metal decreases. This shrinkage is compensated by adding more liquid melt and is referred to as feeding. Common casting defects include shrinkage porosity, which represents areas that cannot be fed sufficiently. These casting defects either make the part unusable or significantly lower the part's quality. Hence, in casting processes such as sand-casting or low-pressure die casting, directed solidification is desirable so that all areas are fed sufficiently and no shrinkage porosity occurs [2,3].

Consequently, when evaluating the casting process for near-net-shape products, both the mold filling and the subsequent solidification of the melt are evaluated for the design of the casting system and, if necessary, to make adjustments to the component geometry. Until now, this evaluation has largely been carried out during the final phase of component design and requires a high level of manual effort to set up and evaluate the simulation. To integrate process knowledge in the early phase

* Corresponding author.
E-mail address: maximilian.erber@utg.de (M. Erber).
[1] These authors contribute equally.

https://doi.org/10.1016/j.cad.2022.103394

of component design, methods are needed that allow a quick evaluation of the geometry. In the past, two method classes were used to evaluate solidification behavior:

- Numerical solidification using the finite volume method (FVM), finite differences method (FDM), or finite element method (FEM)
- Geometrical approaches.

In the first method class, the numerical determination of the solidification time is based on the solving of an unsteady heat conduction equation. In the second method class, the evaluation of solidification behavior is based solely on component geometry under the premise that the geometry is the main factor influencing solidification. In this paper, we use the term geometrical approaches for this class of methods.

2.1. Topology optimization of castings

Among computer-aided engineering tools available for structural optimization, topology optimization (TO) is widely used. It has reached a certain level of maturity in recent years, with fields of application extending from structural and civil engineering to aeronautical and aerospace engineering [4–9].

As TO describes the optimal material distribution in a design space under given loads and constraints, it is commonly used during the initial stage of the product development process [10,11]. However, due to geometric complexity, the results of TO are often non-manufacturable design proposals, which results in extensive redesigning efforts [11–14]. Consequently, the transformation of TO results into editable CAD geometries has become a key research area in recent years in order to reduce the effort needed to redesign or adapt design proposals [15–19]. In addition to the geometry reconstruction of the TO result, it is further desired that the design proposal is dedicated to a particular manufacturing process. Therefore, manufacturing constraints have been incorporated into the TO framework. In terms of casting, these constraints include minimum length scale, symmetry, or extrusion [14,20].

For implementing manufacturing constraints in TO, Vatanabe et al. used a unified projection-based approach, while, for instance, Li et al. applied a virtual temperature method to avoid voids and undercut in the design proposals [14,21]. Particular reference is made to the demolding direction and the parting lines of the mold in the literature for the achievement of castable design proposals [12,20–22]. These methods shrink the design space of an unconstrained TO problem. Therefore, they can be described as significantly narrowing the range of solutions to a TO problem, thereby simplifying the obtained design proposal. Also, these constraints are derived from practical experience of casting design, knowing that the constraints generally improve manufacturing outcomes. Accordingly, these methods essentially describe a simplification of the unconstrained design proposal and are not capable of describing the limits of stable casting processes [23]. Therefore, it may be desirable to incorporate detailed process knowledge into the structural optimization process.

Consequently, Zhao et al. considered that hollow structures generally are more suited for casting processes and used three-dimensional morphable bars to transform solid into hollow structures [24]. Alternatively, the incorporation of casting process simulations can be used to obtain casting design proposals with improved manufacturability [23,25]. For evaluating the manufacturability of areas within the design space, Heilmeier et al. used Djikstra's shortest path algorithm [26] to investigate high-pressure die castings [27]. This simplification allowed fast predictions but neglected the dynamics of the fluid flow as well as the local thickness of the geometry. Alternatively, Rosnitschek et al. used a logarithmic quotient of the solidification time and the distance to the ingate level to evaluate low-pressure die castings [23].

A challenge is then the combination of results from TO and process simulation. Skeletonization techniques are potentially well suited to overcoming this challenge because they intuitively capture meaningful information such as symmetry, local complexity, adjacency, or local width [11,16]. Skeletonization techniques can be sub-divided into surface skeletons, such as the medial axis transform (MAT), or curve skeletons.

While many methods for application to two-dimensional problems can be found in the literature, sources for three-dimensional skeletonization methods are relatively scarce [11,16]. Nevertheless, medial axis skeletons provide the locus of centers of maximally inscribed balls, which represent a solid theoretical basis for the definition of 3D skeletons [16]. Therefore, in Section 3, we describe how to use the medial axis transformation for the geometry-based assurance of directional solidification for complex topology-optimized casting design proposals.

2.2. Geometrical approaches for solidification estimation

The need for geometrical approaches is based on the requirement for low computational cost and to achieve fast decision-making during the design process. The geometric evaluation approach neglects other casting process parameters, such as the heat transfer between mold and component and the thermal characteristics of the mold material and component material. In general, no absolute value is determined as an evaluation criterion but rather a relative value that enables the comparison of different component areas [28]. Based on this relative parameter, local hotspots are then determined, indicating possible positions that cannot be fed, leading to shrinkage cavities.

Most models are based on Chvorinov's rule [29], which proposes the solidification time t_s based on the modulus of a component. The modulus pertains to the ratio of a heat content volume V and the heat transferring area A surrounding this volume. The cast and mold material define the material constant k.

$$t_s = k\left(\frac{V}{A}\right)^2 \tag{1}$$

Many researchers have investigated and proposed derivatives of Chvorinov's rule. The relationship in Eq. (1) can be either used interactively by dividing a casting geometry into simple subcomponents or by approximating the relationship if an intuitive division is not possible. Wlodawer used the first approach and proposed a rule based on the moduli to ensure the function of feeders [2]. The other approach is also known as section modulus and was introduced by Neises et al. [30]. It can be calculated for any point in the cavity by

$$M = \frac{2}{\sum_{i=1}^{N} \frac{1}{d_i}} \tag{2}$$

where N is the number of cooling directions, and d_i is the shortest euclidean distance to the casting surface [31]. Upadhya and Ravi expanded the method for three-dimensional shapes by discretization using a rectangular 3D mesh and introduced methods for further consideration of the casting surface via shape factors or chills [28,31].

Pao, Ransing, and Sood introduced another approach [32–34]. They used the distance transform as an evaluation criterion along the midplane of a casting. This criterion further reduced the number of evaluated samples, identified solidification paths, and optimized the heat transfer coefficients for ensuring directed solidification. Recently, Auger proposed a geometrical modulus calculation based on the evaluation of single Voronoi cells, which

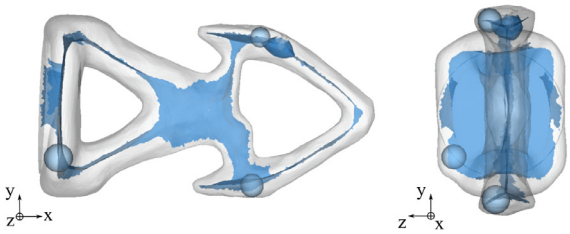

Fig. 1. The medial axis transform of a topology optimized cantilever. Every point on the medial axis transform corresponds to an internal ball, that touches the geometry's surface, but does not cross it. Small features and long additional sheets have been filtered with our method. (For interpretation of the references to color in this figure legend, the reader is referred to the web version of this article.)

allowed the evaluation of complex shapes [35] and Warriner and Monroe used the distance transform for hotspot identification and feeder generation [36].

2.3. Medial axis transform

In the three-dimensional space, the skeleton of a geometry can be described using different methods. One method is to describe the geometry by its midplane, that consists of several surfaces, each describing a feature of the geometry. Other skeleton methods, such as the curve skeleton, describe the geometry by a single curve with corresponding cross-sections for each feature. In this work, we use the medial surface approach to describe our geometries, in order to use the method for different casting geometries including thin-walled high-pressure die castings.

The medial axis transform, also named medial surface, is the skeleton that describes the topology and geometry of an object by the set of maximal balls entirely contained within the object [37]. These skeletons aim to describe the geometric and topological properties of an object in an intuitive way [38]. In the example shown in Fig. 1, the gray surface outlines the volume of a topology-optimized cantilever. The blue surface defines the medial axis transform. The maximum inscribed sphere (light blue) specifies the shortest euclidean distance to the geometry's surface for every point on the medial axis.

There are different ways of calculating the medial axis transform for three-dimensional objects. Mesh-based methods mostly use the Voronoi diagram for the skeletonization [39,40]. Advantages of these algorithms are a low complexity of $\mathcal{O}(n^2)$, the handling of non equally spaced sample points, as well as an easy process for the reconstruction of the medial axis. Voxel-based methods discretize the part's geometry in advance and define the medial axis, for example, by thinning [41,42], distance-field methods [43] or using the interior Voronoi diagram [44]. They can be efficiently calculated in parallel on GPUs, but the reconstruction of the skeleton is a nontrivial problem due to non-manifold and self-intersecting surfaces [45].

A significant disadvantage of the medial axis is its instability. Two very similar objects can have significantly different skeletons, and a rough surface and discretization errors lead to complex medial surfaces with long additional branches or sheets [40]. Therefore, several filtering methods have been proposed, such as angle-based filtering [46–48] using the angle at the medial axis formed by the connection of the contact points and the medial point itself, or distance-based simplification [49] that uses the distance of the contact points corresponding to a medial axis point. Further methods use a volume-based approach [37] or determine the importance based on a scale adaptive classification [40].

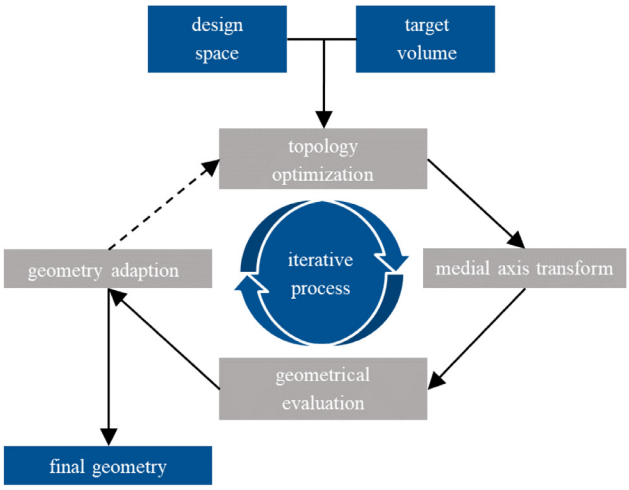

Fig. 2. Workflow for creating topology optimized geometries by incorporating directed solidification. In this work the iterative process has only been performed once.

2.4. Medial axis for casting evaluation

Research on casting process evaluation using the medial axis transform is scarce. Sood, Pao, and Ransing presented the only approach of which the authors are aware [32–34]. Using the commercial software tool CADfix, they calculated the medial axis transform of CAD products and evaluated the solidification time based on the distance to the surface of the casting. By manual definition of solidification paths along the medial axis surface, they determined a local variant heat transfer coefficient to ensure a directed solidification. The validity of this optimization technique is debatable because the opportunity for local adjustment of the heat transfer coefficient during the actual casting process is limited. For this purpose, it would be necessary to apply release layers of different thicknesses or different thermal conductivity to the casting mold locally. In addition, these release layers would also have to be ensured for larger quantities in order to avoid defects and thus rejects. Another difficulty in this approach is the transferability of its method to complex geometries, as they are found in TO. Therefore, some challenges remain unsolved, and the objective of this paper is to provide solutions:

- The evaluation of complex cast components with geometric models has so far only been investigated using voxel-based methods.
- Up until now, it has been necessary to specify the solidification path manually, which prevents its use in automated optimization.
- Up until now, geometrical models have only been used to evaluate geometries but not to optimize the geometry.

3. Proposed method

Our approach shows a possible way for including process requirements in the topology optimization for casting geometries. Our proposed workflow is shown in Fig. 2. The objective of this workflow is to generate a topology-optimized geometry, that allows directional solidification towards the ingate in order to reduce casting defects. Therefore, we included the following topics in this work:

- Generate a surface model produced by topology optimization.

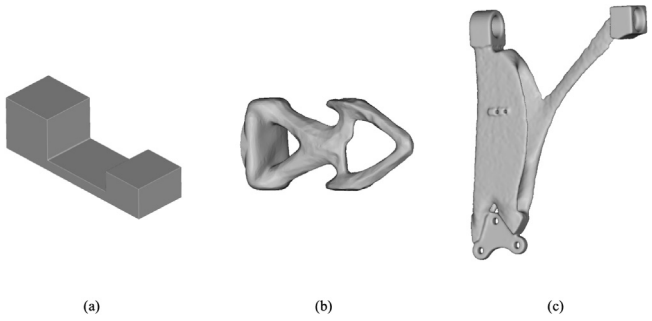

Fig. 3. The three sample geometries, union of cuboids (a), TO results of a cantilever beam (b), a traverse link (c).

- Compute an approximate medial axis transform (MAT) using the Voronoi diagram of a set of equally spaced points on the surface of the geometry.
- Filter the approximate MAT to exclude artifacts like spikes and small features.
- Use the MAT and its radii to identify local thickness maxima. Automatically define directional solidification paths from the ingate towards these maxima.
- Modify the radii along these paths to eliminate local maxima and reconstruct a modified surface shape of the casting.
- Ideally, export a design proposal where the radius decreases monotonically from the ingate of the casting.

The induced error caused by the transformation of the surface of the geometry to the MAT representation and the subsequent transformation back to a geometry surface, is evaluated by measuring the Hausdorff distance [50] in Section 4.3. The Hausdorff distance measures the deviation between the original surface and the reconstructed surface without changing the radii of the medial axis spheres.

As is common in TO, the starting point is the definition of the design space and the target volume defining the mass loss in the design proposal. With this information the TO generates an optimized structural design proposal. Then we integrate our process requirements into this design proposal through a geometry analysis using Python. Hence, we simplify our geometry based on its mid planes using the medial axis transform.

A graph is constructed for the medial axis that allows the identification of material accumulations, also referred to as local hotspots, in the geometry and paths for a directional solidification based on graph theory. By iterative adaption of the geometry along those paths we create a final geometry that is based on the topology-optimized geometry and additionally exhibits better castability. A new surface geometry of the final geometry is exported. Commonly used casting software evaluates the method in terms of prediction accuracy and optimization results.

In this paper, three different geometries, defined by a triangulated surface geometry, shown in Fig. 3, are used as input data.

3.1. Topology optimization

For the TO of the investigated samples, we use the common density-based single isotropic material penalization (SIMP) approach initially described by Bendsoe and Kikuchi [51]. We solve a minimum compliance problem with a volume constraint, which can be formulated as:

$$min\ C = min\ u^T K u, \qquad subject\ to: v \leq V_T \tag{3}$$

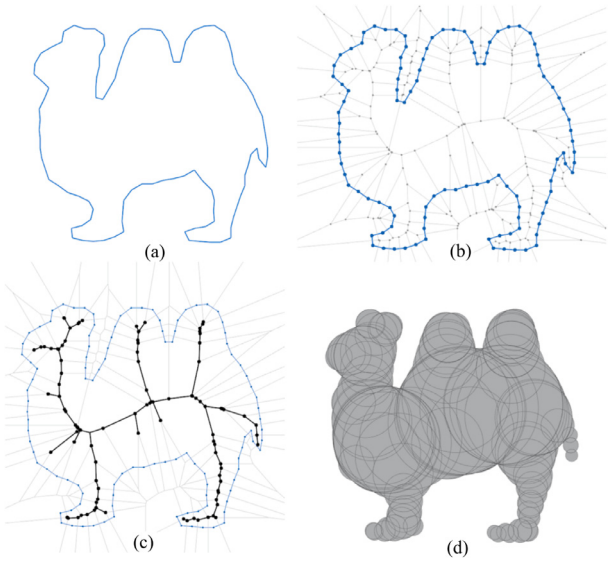

Fig. 4. Schematic creation of medial axis for a 2D shape defined as a polygon (a), the sample points on the polygon and their Voronoi diagram (b). By filtering the Voronoi diagram the medial axis transform is calculated (c). Using the vertices of the medial axis and their shortest distance to the sample a reconstruction of the polygon is possible (d).

where C denotes the compliance, and K and u are the stiffness matrix and displacement vector, respectively. The volume constraint is defined by the relative volume v, which must be less than or equal to the relative target volume V_T.

3.2. Voronoi diagram for medial axis transform

We use a geometrical evaluation and optimization approach implemented in Python [52]. We use the following open-source modules NumPy [53], Pandas [54], Trimesh [55], PyVista [56], SciPy [57], NetworkX [58], pymeshfix [59] and Vedo [60] to complete our work. We used various shapes of the dataset introduced by [61] to test the algorithm in 2D.

Therefore, we use a mesh-based method using the Voronoi diagram for the calculation of the inner medial axis transform of the casting. Fig. 4 shows the schematic creation of the medial axis using the Voronoi diagram for the polygon shown in Fig. 4a. At first a sample P with a specified number of approximately evenly spaced surface points is defined. For the three-dimensional case, this set is not defined by the facet vertices, but uses random points that are approximately evenly spaced on the geometry surface . The Voronoi diagram is calculated for all sample points, see Fig. 4b. This diagram represents a decomposition of the space based on the sample. For each Voronoi region, called a Voronoi cell, the corresponding sample point has the closest distance compared to all other sample points. Voronoi vertices v are the positions in the diagram which have the same distance to at least three sample points in the two-dimensional case, and to at least four sample points in the three-dimensional case. These vertices are linked by edges in the two-dimensional space and additionally by planes in the three-dimensional space. The medial axis transform of an object is defined by the inner vertices of the Voronoi regions and the boundary segments connecting them, shown as black vertices and edges in Fig. 4c. The MAT in combination with the closest distance of every MAT vertex to the sample set contains all information for a reconstruction of the object. Therefore in 2D the reconstructed object is the union of all circles, with the center defined by the MAT vertices and its corresponding closest distance to the sample set, as shown in Fig. 4d.

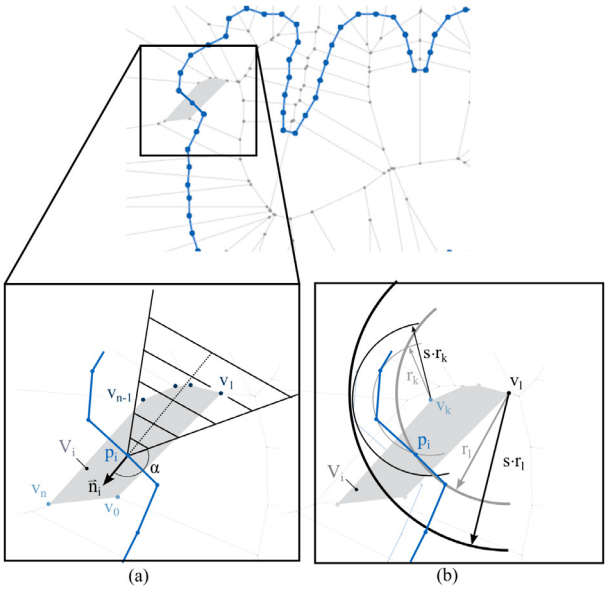

Fig. 5. Geometric filtering methods for extracting the medial axis transform from the Voronoi diagram, shown for a single Voronoi cell V_i. Determining the set of the inner Voronoi vertices by angle filtering (a). Filtering method of small medial axis balls by expansion of balls (b).

3.3. Angle-based filtering of the voronoi diagram

As illustrated in Fig. 4 the skeleton of an object can be described by the subset of the Voronoi diagram, that lies inside an object. Thus, a fast filtering method of the Voronoi diagram is needed to derive this skeleton, therefore we propose a method in this section. The algorithm starts by calculating the Voronoi diagram of the evenly spaced points $p \in P$. A set Z of eight vertices of a large box surrounding the geometry is added to the sample set P. This set Z is neglected for the further filtering and evaluation and only used for computing the Voronoi diagram. The information of the surface mesh facilitates the procedure of filtering the Voronoi diagram of the object. For every point $p \in P$ a normal is derived from the information of the adjacent faces pointing outside of the surface mesh.

For the detection of the inner Voronoi diagram an angle-based filtering method, the pseudo code shown in Algorithm 1, is used. An example of the filtering method is shown in Fig. 5a for a specific Voronoi cell V_i of the two-dimensional polygon. A subset F defines the filtered Voronoi vertices, that should be kept. All vertices that span the Voronoi cell are determined for each Voronoi cell V_i with its corresponding point p_i and normal $\overrightarrow{n_i}$. For every vertex v_j the vector from the current point p_i towards this vertex is calculated, and the angle spanned between the vector $\overrightarrow{p_i v_j}$ and the current normal $\overrightarrow{n_i}$ is determined. If this angle is greater than a predefined angle α, the vertex v_j is added to the set F. This method is repeated for every Voronoi cell and the filtered Voronoi diagram is defined by all vertices that fulfilled the angle criterion in Algorithm 1 at least once. This angle-based method leads to the inner Voronoi diagram. Varying the parameter α allows a first filtering to avoid sharp additional branches and sheets because of rough surfaces of the geometry.

3.4. Simplification of medial axis by expansion of balls

An idea introduced by Miklos is used for the further simplification. The scale adaptive classification relies on a size comparison between a geometry section and its surrounding geometry. If the current section appears small relative to its surroundings, it is proposed as an irrelevant geometry section and therefore ignored. This leads to a new shape containing only the significant features of a geometry [40]. As shown in Fig. 5b the geometry can be represented by the inner Voronoi vertices and their corresponding distance to the geometry's surface. Below, we refer to this representation as medial axis balls, where the ball's midpoint is defined by the Voronoi vertex and the radius of the ball is defined by its shortest euclidean distance to the sample P. By scaling all ball radii with a specified scaling factor s, irrelevant balls will be swallowed by bigger neighboring balls, which increase more, with the same scaling factor s than the irrelevant balls. An example of this is shown in Fig. 5b for the Voronoi cell V_i. The small ball defined by the vertex v_k with the radius r_k will get swallowed by the ball of vertex v_l with the radius r_l, if both radii get expanded by a sufficient high scaling factor s. Whereas Miklos did not define a neighborhood for his simplification method, we define the neighborhood only by the vertices of the surrounding Voronoi cells of the vertex to be observed.

Algorithm 1 Minimum angle filtering.

Input: Sample P, with sample points p and sample normals $\overrightarrow{n}$, filtering angle α

Compute V_P
$F = \emptyset$
for $V_i \in$ Voronoi cells V **do**
  Get sample point $p_i \in P$
  Get normal $\overrightarrow{n_i}$
  Get Voronoi vertices $v \in V_i$
  for each $v_j \in v$ **do**
    Compute $\overrightarrow{p_i v_j}$
    if $\angle(\overrightarrow{n_i}, \overrightarrow{p_i v_j}) > \alpha$ **then**
      $F = F \cup \{v_j\}$
    end if
  end for
end for

Output: Filtered Voronoi vertices F

Algorithm 2 Filtering by expansion of balls.

Input: Sample P, Filtered Voronoi vertices F, Voronoi diagram V_P,

$F_{final} = copy(F)$
$F_{delete} = \emptyset$
Calculate distance to sample: $r(f \in F) = \min_{p \in P} \|f - p\|$
Calculate expanded distance: $r_{exp} = s \cdot r$
for each Voronoi cell $V_i \in V_P$ **do**
  Get subset of inner Voronoi vertices
  $v_{in} = F \cap (v \in V_i)$
  for each $v_k \in v_{in}$ **do**
    $v_{others} = v_{in} \setminus v_k$
    if $r_{exp,others} > (r_{exp,k} + \|v_{others} - v_k\|)$ **then**
      $F_{delete} = F_{delete} \cup \{v_k\}$
    end if
  end for
end for

while Vertices in F_{delete} on border of MAT: **do**
  for $v_{check} \in F_{delete}$ **do**
    if v_{check} on border of MAT: **then**
      $F_{final} = F_{final} \setminus \{v_{check}\}$
      $F_{delete} = F_{delete} \setminus \{v_{check}\}$
      Update MAT
    end if
  end for
end while

Output: Final filtered Voronoi vertices F_{final}

The pseudo code is shown in Algorithm 2. The filtered Voronoi diagram F, the sample P, the initial Voronoi diagram V_P and a

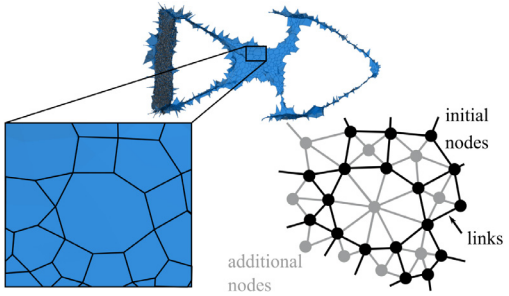

Fig. 6. Transformation of MAT to a graph with additional nodes for surfaces with more than three vertices for higher precision of shortest path calculations. Due to a low number of 2000 sample points the smoothness of the medial axis decreases and there is an increased number of long additional branches due to discretization errors.

predefined scaling factor s are required for this. For every filtered vertex $f \in F$ the radius, defined by the minimal euclidean distance to the sample P, is determined and multiplied by the scaling factor s. The filtering method is applied to the subset of all inner vertices of the Voronoi cell. Therefore, the inner vertices are split into the current vertex v_k and all other vertices v_{other}. If the condition that any of the other ball radii is greater than the sum of the expanded ball radius $r_{exp,k}$ and the distance of this vertex towards vertex v_k is true, vertex v_k will be proposed as irrelevant and therefore be included in a set of points F_{delete}, that should be deleted.

The structure of the Voronoi diagram in combination with the filtered Voronoi vertices allows a mesh-based approximation of the medial axis. Thus, the Voronoi diagram for a three-dimensional point cloud has Voronoi vertices as well as Voronoi edges and Voronoi surfaces. Edges in the diagram represent positions in space that have an equal distance to three sample points and are limited by two Voronoi vertices, while faces have the same distance to two sample points. This information can be used to approximate the medial axis by filtering the remaining Voronoi surfaces. Only surfaces whose boundary points are all a subset of F_{final} are kept. Again, only edges that run along these faces are considered as edges of the medial axis.

In a subsequent iterative process only those points are deleted that satisfy the condition of being in the set of F_{delete} and lying on the border of the medial axis to prevent the formation of holes in the medial axis surface and to ensure its connectivity. The condition of lying on the MAT border is satisfied if a point has only one adjacency face.

3.5. Evaluation of the medial axis

The medial axis calculation is followed by a graph-based evaluation of the medial axis transform. The nodes of these graphs are defined by the filtered Voronoi vertices, the links between the vertices by the remaining edges. Since the number of vertices of the Voronoi surface varies, as shown in Fig. 6, in our method surfaces with more than three vertices were additionally decomposed into triangles by additional midpoints and links between each vertex and midpoint. On the one hand this leads to more precise shortest path calculations and our MAT can be further edited using modules designed for triangulated meshes. Hotspots, which would potentially lead to shrinkage porosity in the event of insufficient feeding, are derived from local maxima of the radius in the graph. An additional prominence criterion allows further filtering of the hotspots. This criterion checks for each local maximum whether its radius is larger than the radii of all adjacency nodes within a given range along the graph.

Shrinkage porosity can be avoided by ensuring sufficient feeding at local material accumulations. This can be achieved on the one hand by feeding via the ingate of the component or by additional feeders placed at the component surface. In our work, directional solidification was to be achieved exclusively via an isolated ingate, analogous to the process in low-pressure die casting, in order to keep the model complexity low. Therefore, the ingate is placed at the thickest section of the part. As a criterion for sufficient feeding, we propose that every position in the part must be reachable along a path from the ingate with a decreasing thickness. Hotspots do not fulfill this criterion. Therefore for every hotspot the shortest path [26] weighted by the edge lengths along the graph towards the ingate is calculated, and in a second step all balls along this path are expanded until no more local maxima are found except the ingate. This shape modification of the MAT ensures the manufacturability with less casting defects caused by shrinkage.

3.6. Reconstruction of optimized geometry

We use a discretization method by voxelization for the reconstruction of the optimized structure defined by the adapted MAT. For this purpose, the space of the bounding box with an additional user defined offset is partitioned into equally spaced voxels defined by their edge length, also referred to as voxel size. Then, for each Voronoi sphere, all voxel centers located in the sphere's domain are identified. The final volume is defined as the union of all identified voxels of all Voronoi spheres. From this, the faces between inside and outside voxels are determined by Boolean comparison of adjacency voxels. These surfaces get triangulated, taking into account the normal direction pointing outside the geometry. Then, the generated surface is reduced to its largest connected component by describing it as a graph, where the nodes of the graph are defined by the triangles and the edges of the triangles represent the links in the graph.

Graph methods are then used to find non-manifold edges and the points representing these edges are deleted. The resulting holes are closed using existing functions of the pymeshfix module [59]. We obtain a watertight mesh that can further be used in CAD tools or simulation environments. The surface is smoothed using a Laplacian method and can be exported as a surface object using the standard file format .stl that is supported for many software packages.

4. Results

4.1. Medial axis calculation

In order to use the surrogate model of the medial axis transformation for the evaluation and optimization of cast components, a stable and sufficiently accurate model transfer for arbitrary geometries and components must be ensured. Since topology-optimized components can have complex surfaces, the geometry (dimensions 160 x 50 x 50 mm) in Fig. 3a with different rough surfaces was examined as an endurance test. The geometries as well as their medial axis transformation are shown in Fig. 7.

For this purpose, the component was meshed with 20,000 sample points. These points were then randomly shifted firstly with a small displacement of up to 0.1% of the component diagonal (Õ.17 mm) and then secondly with a high displacement in a range of up to 1% (1.7 mm). This displacement was sufficiently high to generate overlaps of individual surfaces. These geometries were used to estimate the limits of the angle filtering method for rough surfaces. The test investigated the stability of the significant surfaces of the skeleton. For the evaluation, a filtering

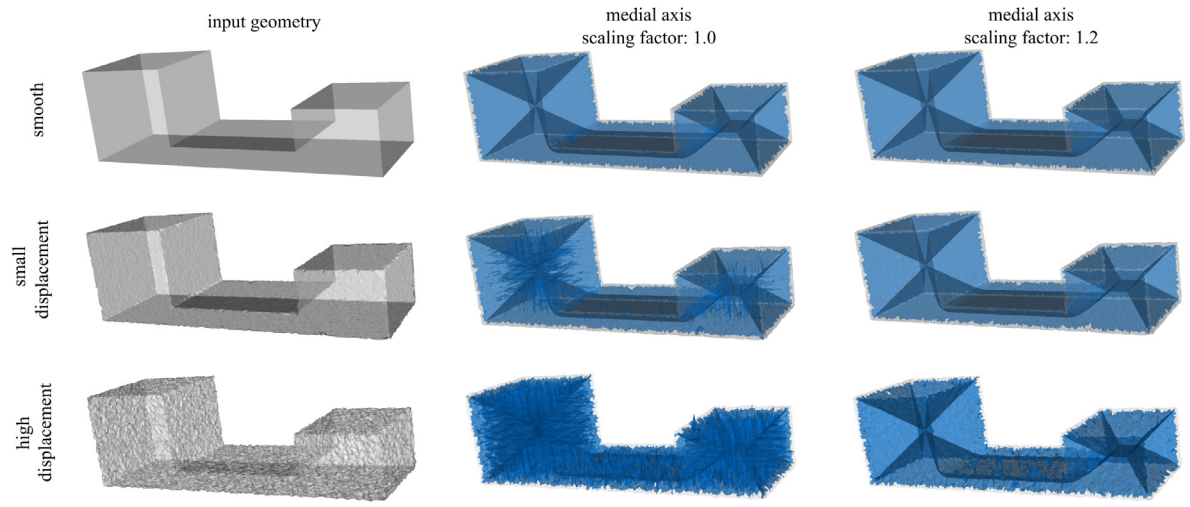

Fig. 7. Medial axis transformation for a geometry with randomized displaced surface vertices.

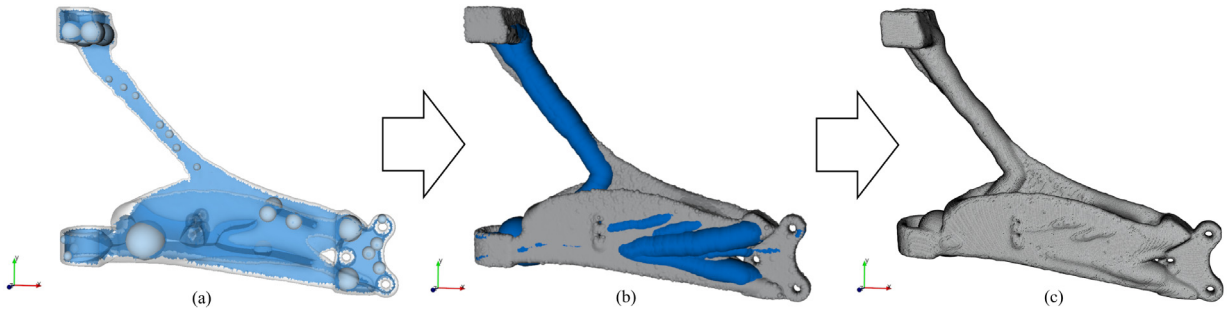

Fig. 8. Detection of the local maxima in the structure, shown by way of example for the traverse link. These local maxima represent hotspots, which lead to potential shrinkage porosity. The hotspots are visualized as light blue spheres in the figure. These hotspots are subsequently reduced to obtain an optimized design geometry. (a) The central figure shows the union of balls defined by the MAT of the initial geometry (gray). Sections with expanded balls modified by the optimization are marked in blue. (b) The right figure shows the reconstructed watertight surface mesh, which can be used in other software tools (c). (For interpretation of the references to color in this figure legend, the reader is referred to the web version of this article.)

angle of 135 degrees and scaling factors of 1.0 for no filtering by expansion and 1.2 for filtering was used.

For the smooth input geometry, an angle-based filtering of the Voronoi diagram is sufficient to generate the significant medial axis transformation. Good results are obtained with a filtering angle α of 135°. Too small angles lead to an incorrect classification of few outer vertices. These errors mainly occur at sharp edges of the geometry. An angle greater than 160° filters the MAT too drastically, resulting in incomplete connectivity of the medial axis. An increased scaling factor clears only some vertices at the inside edges of the input geometry. Small displacements of the sample points lead to some long additional branches, but no outer vertices are classified incorrectly. By using a scaling factor of 1.2 the significant features of the medial axis are highlighted. If the displacements are too high, the actual medial surface is difficult to recognize after the angle-based filtering and individual points that lie outside the component are classified as interior points. Nevertheless, the basic skeleton of the component can be constructed with the help of further filtering.

4.2. Hot spot detection of initial and optimized part

By transferring the geometry into a graph, we can use it to detect potential hot spots in the structure, which may lead to shrinkage porosity in the castings. For this purpose, we can use the radii of the medial axis points that provide information about the geometric entities. Since, in the case of directional solidification, geometries that are conical along the solidification path are favorable, the radii of the points should decrease. Hence, thicker areas should be near the ingate to avoid shrinkage porosity or areas that cannot be filled due to premature solidification. Consequently, we can define local maxima as any point on the medial axis graph with a greater radius than its adjacent neighborhood. We defined this neighborhood by a distance of 15 mm to the local maximum along the graph. These local maxima represent potential hotspots. For example, the hotspots of the traverse arm can be seen as light blue spheres within the volume in Fig. 8. In the example shown in Fig. 8 the filtering reduces the number of hotspots from 600 to 25. The optimization of these 25 maxima is sufficient, because many local maxima are only due to discretization errors and therefore do not have a large impact on the optimization results. The final geometry is exported in a standard file format as a surface mesh, as shown in Fig. 8c.

4.3. Reconstruction quality

In this section we present the results of the quality of the reconstruction of the medial axis transform to a surface model. To obtain the results, we calculated the medial axis transform of our example surface models with 20,000 and 100,000 sample points and reconstructed their non optimized surface. For the evaluation of the reconstruction quality we calculated the Hausdorff [50] distance of the new reconstructed geometry's surface based on the input geometry's surface. Therefore, we used the vertices of the new surface as the sample for the Hausdorff distance. These

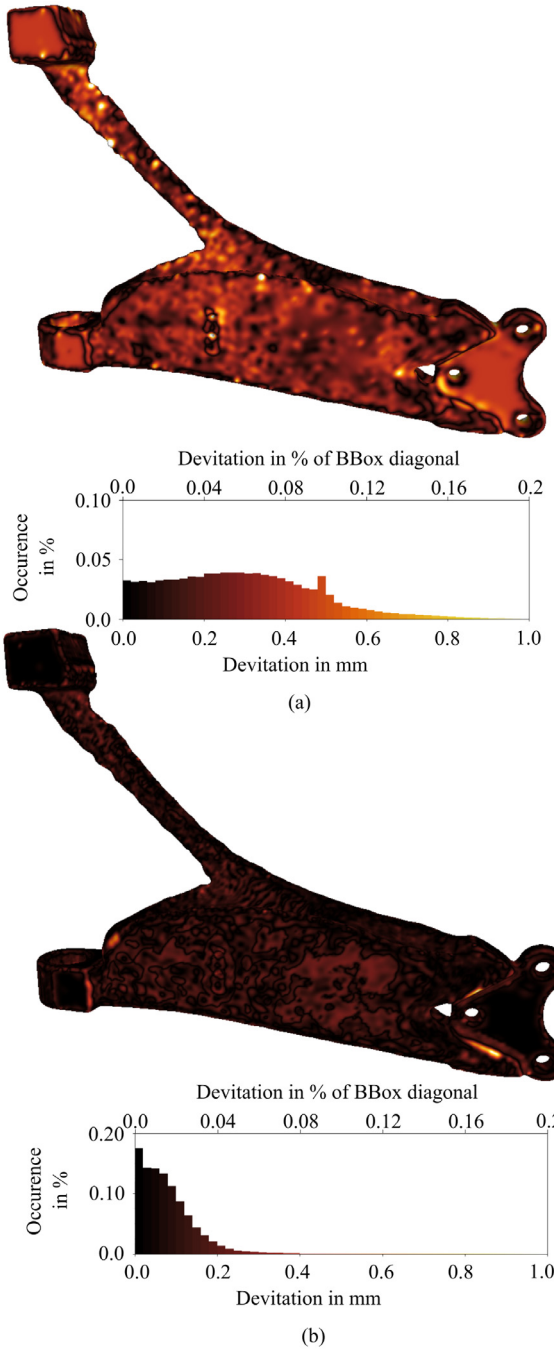

Fig. 9. Hausdorff-Distance of reconstructed geometry. (a) Medial axis calculation with 20,000 sample points and reconstruction with a voxel size of 1 mm. (b) Medial axis calculation with 100,000 sample points and reconstruction with a voxel size of 0.5 mm.

results are shown in Fig. 9, where dark faces of the mesh indicate a small deviation between those two meshes and brighter faces indicate higher deviations. For a better visualization, the histogram shows only values in a range of 0 to 1 mm, deviations of more than 1 mm are considered in the 1 mm bin. In Fig. 9a the medial axis was calculated using 20,000 sample points and a reconstruction with a voxel size of 1 mm. The maximum Hausdorff distance is 4.2 mm, but only 1.5% of the new surface vertices have a distance of more than 1 mm to the original geometry. The mean deviation is 0.3 mm, which is about 0.06% of the bounding box diagonal (BBox diagonal). If the number of

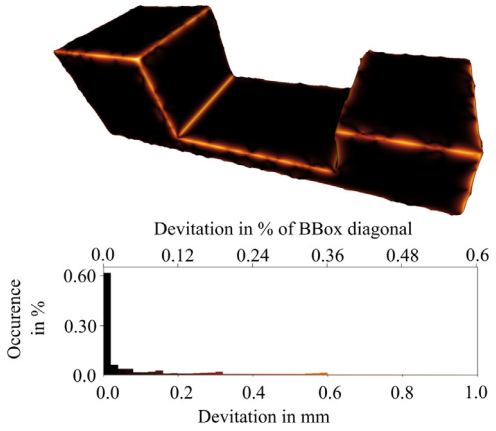

Fig. 10. Hausdorff-Distance of reconstructed geometry with 20,000 sample points and reconstruction with a voxel size of 1 mm.

samples for the construction of the medial axis is increased and the voxel mesh is refined as demonstrated in Fig. 9b for 100,000 sample points, the accuracy of the new mesh can be further improved, which results in a maximum deviation of 1.2 mm and a mean deviation of 0.07 mm. As shown in Fig. 10 these maximal deviations mainly occur on sharp edges of the original geometry due to the reconstruction using spheres.

4.4. Adaption of part geometry

The optimization method was evaluated by adapting two topology-optimized geometries shown in Fig. 3b and c. Because the example of the traverse link has a much more complex geometry, this example will be used to validate the methodology in the further course.

The medial axis transformation provides a stable medial axis even for complex topology-optimized structures, which we use to define the directional solidification path. In combination with hotspot detection and the shortest path, we can evaluate the castability of the design proposal using geometry-based criteria. Hence, the proposed method provides us data based on geometrical criteria, where adding additional material in the design space increases the manufacturability by minimizing the risk of potential casting defects. Fig. 8b shows the final geometry, with expanded sections are marked in blue.

In particular, the initial design space volume of the traverse link example is reduced by TO to 39.05%. This topology-optimized geometry is shown in gray in Fig. 8b. After the medial axis transformation and hotspot detection, 9.47% of the initial volume, marked as blue, is again added to prevent shrinkage porosity in the casting leading to a final volume of 48.52% of the initial casting, shown as blue in Fig. 8. This addition of material is mainly due to expansion of medial balls along the shortest paths between ingate and detected hotspots because a simple reconstruction of the traverse link without solidification path optimization leads to a relative change of the volume of +1.32%.

4.5. Calculation times

The calculation times for the three geometries in Fig. 3 are listed in Table 1. For the filtering an angle of 135 degree and an expansion factor of 1.2 were used. The calculation times are most influenced by the number of sample points, respectively the number of MAT vertices.

Table 1
Performance in seconds for medial axis calculation, the evaluation and geometry adaption for better castability and the final surface reconstruction.

Model	Points (sample)	Voxel size (mm)	Number voxels	Vertices MAT	MAT creation (s)	Evaluation (s)	Reconstruction (s)
Union of cuboids	20,000	1.0	714,432	63,040	23.48	–	40.78
Cantilever	20,000	1.0	373,527	46,205	14.82	58.36	5.67
Traverse link	20,000	1.0	12,465,484	62,003	18.25	64.09	70.06
Traverse link	100,000	0.5	98,876,988	300,189	120.29	560.89	2137.16

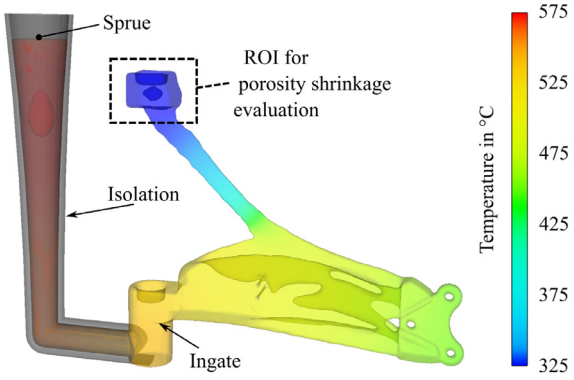

Fig. 11. Casting process simulation of solely topology-optimized traverse link at 1200 s after start of filling. The region of interest (ROI) shows the non-feedable geometry section. The surrounding mold is not shown in the figure.

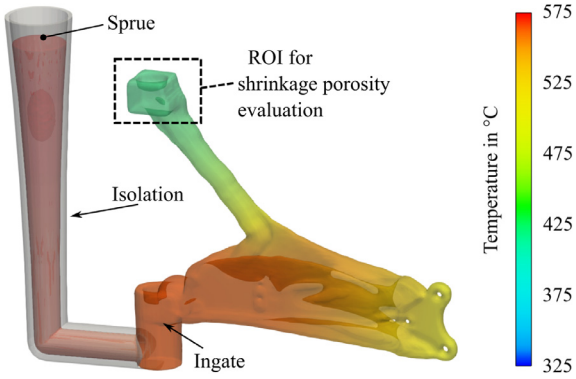

Fig. 12. Casting process simulation of topology-optimized and process-optimized traverse link at 1200 s after start of filling.

5. Validation method

The geometry modification method in this work was evaluated using a widely used casting process simulation. The simulation was performed using Flow-3D software (v5.0 Update 4, Flow Science Inc., Rottenburg, Germany). Due to the focus on the prevention of shrinkage defects, a mold filling simulation and a subsequent solidification simulation are calculated using FVM. We used a sand casting process for the validation. Mold filling takes place via a sprue and the melt enters the mold via a gating system at the thickest part of the component. The orientation of the casting was chosen to allow a controlled rising filling. The placement and design of the gating system as well as the orientation of the geometry in the mold is essential for the temperature distribution after the filling process and the heat fluxes during the solidification. The temperature distribution at the end of the mold filling is used as boundary condition for the solidification simulation. In this research, the gating system is insulated to prevent early solidification in the gating system and sprue. Therefore, feeding via the casting system is ensured.

For the topology-optimized geometry without a modification for better castability the link between the main body and the upper functionally necessary non-design space, marked as region of interest (ROI) in Fig. 11, solidifies faster than the non-design space. This results in a shrinkage porosity with a volume of 3942.1 mm^3. In the simulation of the modified casting geometry shown in Fig. 12 the volume of this shrinkage porosity can be significantly reduced by 89.4% to a volume of 416.4 mm^3, but cannot be avoided completely. This is due to our optimization criterion of solely estimating the solidification time by the distance transform and neglecting heat dissipation along other directions.

6. Discussion

The results show that the presented approach addresses all three open points listed in Section 2.4. As demonstrated, the presented mesh-based approximation of the medial axis gives stable results for arbitrary complex geometries and rough surfaces as they often result from TO. Hence the method is applicable for the evaluation of arbitrary casting geometries. Due to the use of the Voronoi diagram, the medial axis of the casting geometry can be accurately determined. The mean deviation of 0.06%, respectively a mean deviation of 0.3 mm, relative to the reference geometry for a sample size of 20,000 is acceptable in most cases.

Furthermore, by using the mesh-based approach, we can automatically specify the directed solidification paths by calculating the shortest path along the medial axis. Therefore, the path's edge weights are expressed by the euclidean length of each edge. This is an easy approach for the optimization, but further optimization criteria could be added by changing the edge weights. This allows the model to be used in automated optimization loops. Pao, Ransing, and Sood defined the solidification path manually, therefore, our method represents an improvement on the state-of-the-art and makes the medial axis transform applicable to arbitrary three-dimensional casting geometries with an automated directional solidification modification.

While other approaches only evaluate casting geometries, our approaches presents a method for modifying and optimizing the casting geometry. A final surface mesh is generated and then be subsequently used in CAD and simulation software. The geometry is changed only in areas that are necessary for directional solidification. By increasing the volume by 9.45%, shrinkage porosity present in the component can be reduced by 89.4%. However, complete prevention is not yet possible. We correlated the solidification time with the closest distance to the geometry's surface. Chvorinov and Neises' rules, see Section 2.2, provide further evaluation criteria that estimate the solidification by a sectional modulus of the casting. Our method is not restricted to the distance to surface as an evaluation criterion and can be easily adopted for more complex metrics. Therefore, our aim in our future work is to expand the local solidification approximation using ray tracing methods and integrate the approach of Neises et al. [30]. By integrating these methods in the medial axis model, the accuracy of the solidification time could be approved, enabling the avoidance of further shrinkage defects. Further the temperature distribution after the filling process is not included in any of the proposed methods. By now this distribution can only be calculated by using computationally expensive fluid dynamics calculations. Our aim is to connect these filling simulations with data-driven methods. One interesting additional finding is that

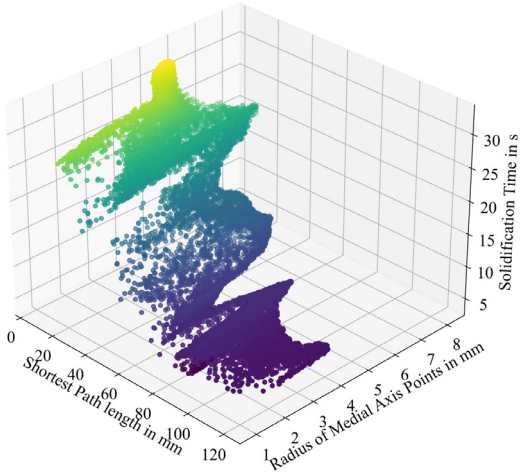

Fig. 13. Correlation between shortest path, medial axis radius and solidification time. The data of the cantilever geometry in 3.b, which is used for a neural network is shown.

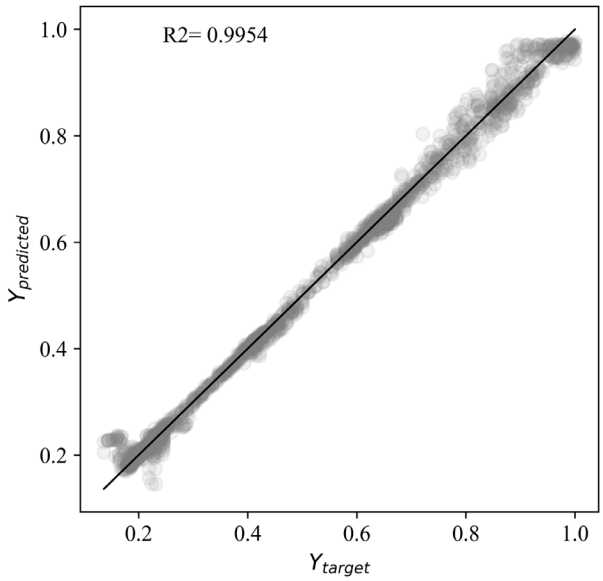

Fig. 14. By using the shortest path values and the radii of the medial axis points as inputs for a neural network, the solidification time can be predicted nearly perfectly for the cantilever beam shown in Fig. 3b.

we observed a certain correlation for the shortest path, the radii of the medial axis points, and the solidification time, as depicted in Fig. 13.

In a first trial, we trained a neural network using TensorFlow [62] with one normalization layer and three dense layers with 64, 128 and 64 neurons, and a ReLU activation for predicting the solidification time of the cantilever beam example (3.b). The model was built so that the solidification time of each mid point is predicted based on its shortest path length to the ingate along the MAT and the radius of the medial axis point; for the data a train-test split of 80% to 20% was used. After training the model for 2000 epochs, it achieved a coefficient of determination (R2) on the test data of 99.54%, as shown in Fig. 14. Therefore, we conclude that we can use this correlation to develop metamodels for predicting the solidification time in die castings and so replacing the time-consuming casting process simulations within a structure-process-optimization framework. Consequently, this will be the main subject of our future work.

As the comparison to the solidification simulation shows, we cannot omit a casting simulation as a final evaluation and process assurance tool, but for iterations within the optimization process in Fig. 2 we can use our method to reduce the geometry evaluation time significantly. In the traverse link example, we could shorten the time for the solidification evaluation by 98% from 180 min to 2.5 min. Hence, a high-quality process assurance cannot be achieved with our model. Instead, the current state of our method can best be described as evaluation of casting geometries and geometry modification for better manufacturability in view of directed solidification of the design proposal.

7. Conclusion

This paper has presented a method for evaluation and optimization of the geometry of castings for directional solidification, which automatically defines the solidification paths and reduces the shrinkage porosity within an arbitrary complex design proposal. For this purpose, we have introduced a mesh-based model for a parametric description of the geometry along its mid plane. The proposed method eliminated nearly the entire shrinkage porosity volume within the design proposals in a few minutes. Therefore, the method can be used for automating structure-process optimization frameworks for castings. The correlation of the shortest path distance and radius of medial axis points shows potential for further research in the field of geometric casting evaluation.

CRediT authorship contribution statement

Maximilian Erber: Conceptualization, Methodology, Software, Validation, Formal analysis, Investigation, Resources, Writing – original draft preparation, Visualization. **Tobias Rosnitschek:** Conceptualization, Methodology, Software, Validation, Formal analysis, Investigation, Resources, Writing – original draft preparation, Visualization. **Christoph Hartmann:** Data curation, Writing – original draft preparation, Writing – review and editing, Supervision. **Bettina Alber-Laukant:** Formal analysis, Data curation, Writing – review and editing, Supervision. **Stephan Tremmel:** Data curation, Writing – review and editing, Supervision, Project administration, Funding acquisition. **Wolfram Volk:** Data curation, Writing – review and editing, Supervision, Project administration, Funding acquisition.

Declaration of competing interest

The authors declare that they have no known competing financial interests or personal relationships that could have appeared to influence the work reported in this paper.

Acknowledgment

All authors have read and agreed to the published version of the manuscript.

Funding

The authors would like to thank the German Research Foundation for financial support under Grant Number 434348474.

References

[1] Li C, Kim IY. Topology, size and shape optimization of an automotive cross car beam. Proc Inst Mech Eng D 2015;229(10):1361–78. http://dx.doi.org/10.1177/0954407014561279.

[2] Wlodawer R. Directional solidification of steel castings. Oxford: Pergamon Press; 1966.

[3] Shahane S, Aluru N, Ferreira P, Kapoor SG, Vanka SP. Finite volume simulation framework for die casting with uncertainty quantification. Appl Math Model 2019;74:132–50. http://dx.doi.org/10.1016/j.apm.2019.04.045, URL: https://linkinghub.elsevier.com/retrieve/pii/S0307904X19302483.

[4] Tsavdaridis KD, Kingman JJ, Toropov VV. Application of structural topology optimisation to perforated steel beams. Comput Struct 2015;158:108–23. http://dx.doi.org/10.1016/j.compstruc.2015.05.004, URL: https://linkinghub.elsevier.com/retrieve/pii/S0045794915001418.

[5] Calabrese M, Primo T, Del Prete A. Optimization of machining fixture for aeronautical thin-walled components. Proc CIRP 2017;60:32–7. http://dx.doi.org/10.1016/j.procir.2017.02.008, URL: https://linkinghub.elsevier.com/retrieve/pii/S2212827117300732.

[6] Ismail AY, Na G, Koo B. Topology and response surface optimization of a bicycle crank arm with multiple load cases. Appl Sci 2020;10(6):2201. http://dx.doi.org/10.3390/app10062201, URL: https://www.mdpi.com/2076-3417/10/6/2201.

[7] Klippstein H, Hassanin H, Diaz De Cerio Sanchez A, Zweiri Y, Seneviratne L. Additive manufacturing of porous structures for unmanned aerial vehicles applications. Adv Energy Mater 2018;20(9):1800290. http://dx.doi.org/10.1002/adem.201800290, URL: https://onlinelibrary.wiley.com/doi/10.1002/adem.201800290.

[8] Larsen U, Signund O, Bouwsta S. Design and fabrication of compliant micromechanisms and structures with negative Poisson's ratio. J Microelectromech Syst 1997;6(2):99–106. http://dx.doi.org/10.1109/84.585787, URL: http://ieeexplore.ieee.org/document/585787/.

[9] Shi G, Guan C, Quan D, Wu D, Tang L, Gao T. An aerospace bracket designed by thermo-elastic topology optimization and manufactured by additive manufacturing. Chin J Aeronaut 2019;S1000936119303358. http://dx.doi.org/10.1016/j.cja.2019.09.006, URL: https://linkinghub.elsevier.com/retrieve/pii/S1000936119303358.

[10] Zuo K-T, Chen L-P, Zhang Y-Q, Yang J. Manufacturing- and machining-based topology optimization. Int J Adv Manuf Technol 2006;27(5–6):531–6. http://dx.doi.org/10.1007/s00170-004-2210-8, URL: http://link.springer.com/10.1007/s00170-004-2210-8.

[11] Nana A, Cuillière J-C, Francois V. Automatic reconstruction of beam structures from 3D topology optimization results. Comput Struct 2017;189:62–82. http://dx.doi.org/10.1016/j.compstruc.2017.04.018, URL: https://linkinghub.elsevier.com/retrieve/pii/S0045794916308835.

[12] Rosnitschek T, Hentschel R, Siegel T, Kleinschrodt C, Zimmermann M, Alber-Laukant B, Rieg F. Optimized one-click development for topology-optimized structures. Appl Sci 2021;11(5):2400. http://dx.doi.org/10.3390/app11052400, URL: https://www.mdpi.com/2076-3417/11/5/2400.

[13] Da D, Xia L, Li G, Huang X. Evolutionary topology optimization of continuum structures with smooth boundary representation. Struct Multidiscip Optim 2018;57(6):2143–59. http://dx.doi.org/10.1007/s00158-017-1846-6, URL: http://link.springer.com/10.1007/s00158-017-1846-6.

[14] Vatanabe SL, Lippi TN, Lima CRd, Paulino GH, Silva EC. Topology optimization with manufacturing constraints: A unified projection-based approach. Adv Eng Softw 2016;100:97–112. http://dx.doi.org/10.1016/j.advengsoft.2016.07.002, URL: https://linkinghub.elsevier.com/retrieve/pii/S0965997816301703.

[15] Koguchi A, Kikuchi N. A surface reconstruction algorithm for topology optimization. Eng Comput 2006;22(1):1–10. http://dx.doi.org/10.1007/s00366-006-0023-0, URL: http://link.springer.com/10.1007/s00366-006-0023-0.

[16] Cuillière J-C, François V, Nana A. Automatic construction of structural CAD models from 3D topology optimization. Comput-Aided Des Appl 2018;15(1):107–21. http://dx.doi.org/10.1080/16864360.2017.1353726, URL: http://www.cad-journal.net/files/vol_15/Vol15No1.html.

[17] Gao Y, Guo Y, Zheng S. A NURBS-based finite cell method for structural topology optimization under geometric constraints. Comput Aided Geom Design 2019;72:1–18. http://dx.doi.org/10.1016/j.cagd.2019.05.001, URL: https://linkinghub.elsevier.com/retrieve/pii/S0167839619300445.

[18] Marinov M, Amagliani M, Barback T, Flower J, Barley S, Furuta S, Charrot P, Henley I, Santhanam N, Finnigan GT, Meshkat S, Hallet J, Sapun M, Wolski P. Generative design conversion to editable and watertight boundary representation. Comput Aided Des 2019;115:194–205. http://dx.doi.org/10.1016/j.cad.2019.05.016, URL: https://linkinghub.elsevier.com/retrieve/pii/S0010448519301873.

[19] Jiu L, Zhang W, Meng L, Zhou Y, Chen L. A CAD-oriented structural topology optimization method. Comput Struct 2020;239:106324. http://dx.doi.org/10.1016/j.compstruc.2020.106324, URL: https://linkinghub.elsevier.com/retrieve/pii/S0045794920301279.

[20] Wang Y, Kang Z. Structural shape and topology optimization of cast parts using level set method: Structural shape and topology optimization of cast parts using level set method. Internat J Numer Methods Engrg 2017;111(13):1252–73. http://dx.doi.org/10.1002/nme.5503, URL: http://doi.wiley.com/10.1002/nme.5503.

[21] Li Q, Chen W, Liu S, Fan H. Topology optimization design of cast parts based on virtual temperature method. Comput Aided Des 2018;94:28–40. http://dx.doi.org/10.1016/j.cad.2017.08.002, URL: https://linkinghub.elsevier.com/retrieve/pii/S0010448517301434.

[22] Sato Y, Yamada T, Izui K, Nishiwaki S. Manufacturability evaluation for molded parts using fictitious physical models, and its application in topology optimization. Int J Adv Manuf Technol 2017;92(1–4):1391–409. http://dx.doi.org/10.1007/s00170-017-0218-0, URL: http://link.springer.com/10.1007/s00170-017-0218-0.

[23] Rosnitschek T, Erber M, Hartmann C, Volk W, Rieg F, Tremmel S. Combining structural optimization and process assurance in implicit modelling for casting parts. Materials 2021;14(13):3715. http://dx.doi.org/10.3390/ma14133715, URL: https://www.mdpi.com/1996-1944/14/13/3715.

[24] Zhao Y, Hoang V-N, Jang G-W, Zuo W. Hollow structural topology optimization to improve manufacturability using three-dimensional moving morphable bars. Adv Eng Softw 2021;152:102955. http://dx.doi.org/10.1016/j.advengsoft.2020.102955, URL: https://linkinghub.elsevier.com/retrieve/pii/S0965997820310012.

[25] Franke T, Fiebig S, Bartz R, Vietor T, Hage J, vom Hofe A. Adaptive topology and shape optimization with integrated casting simulation. In: Rodrigues H, Herskovits J, Mota Soares C, Araújo A, Guedes J, Folgado J, Moleiro F, Madeira JFA, editors. EngOpt 2018 proceedings of the 6th international conference on engineering optimization. Cham: Springer International Publishing; 2019, p. 1263–77. http://dx.doi.org/10.1007/978-3-319-97773-7_109, URL: http://link.springer.com/10.1007/978-3-319-97773-7_109, ISBN:978-3-319-97772-0 978-3-319-97773-7.

[26] Dijkstra EW. A note on two problems in connexion with graphs. Numer Math 1959;1(1):269–71. http://dx.doi.org/10.1007/BF01386390, URL: http://link.springer.com/10.1007/BF01386390.

[27] Heilmeier F, Goller D, Opritescu D, Thoma C, Rieg F, Volk W. Support for ingate design by analysing the geometry of high pressure die cast geometries using Dijkstra's shortest path algorithm. Adv Mater Res 2016;1140:400–7. http://dx.doi.org/10.4028/www.scientific.net/AMR.1140.400, URL: https://www.scientific.net/AMR.1140.400.

[28] Ravi B, Srinivasan MN. Casting solidification analysis by modulus vector method. Int J Cast Met Res 1996;9(1):1–7. http://dx.doi.org/10.1080/13640461.1996.11819638.

[29] Chvorinov N. Theorie der erstarrung von gussstücken. Giesserei 1940;177–86.

[30] Neises SJ, Uicker JJ, Heine RW. Geometric modeling of directional solidification based on section modulus. AFS Trans 1987;(95):25–30.

[31] Upadhya GK, Das S, Chandra U, Paul AJ. Modelling the investment casting process: a novel approach for view factor calculations and defect prediction. Appl Math Model 1995;19(6):354–62. http://dx.doi.org/10.1016/0307-904X(95)90001-O.

[32] Pao W, Ransing R, Lewis R, Lin C. A medial-axes-based interpolation method for solidification simulation. Finite Elem Anal Des 2004;40(5–6):577–93. http://dx.doi.org/10.1016/S0168-874X(03)00097-0.

[33] Ransing RS, Sood MP, Pao W. Computer implementation of Heuvers' circle method for thermal optimisation in castings. Int J Cast Met Res 2005;18(2):119–28. http://dx.doi.org/10.1179/136404605225022910.

[34] Sood MP. A novel geometry based approach for casting process optimisation (Ph.D. thesis), Swansea: Swansea University; 2006.

[35] Auger J-M. Local definition for surface-based geometrical modulus and use in automated casting cooling determination. Int J Cast Met Res 2017;30(6):322–36. http://dx.doi.org/10.1080/13640461.2017.1312737.

[36] Warriner WE, Monroe CA. Open-source MATLAB code for hotspot identification and feeder generation. Int J Metalcast 2019;13(4):793–816. http://dx.doi.org/10.1007/s40962-019-00316-1.

[37] Tam R, Heidrich W. Shape simplification based on the medial axis transform. In: IEEE transactions on ultrasonics, ferroelectrics and frequency control. IEEE; 2003, p. 481–8. http://dx.doi.org/10.1109/VISUAL.2003.1250410.

[38] Giesen J, Miklos B, Pauly M, Wormser C. The scale axis transform. In: Hershberger J, Fogel E, editors. Proceedings of the 25th annual symposium on computational geometry - SCG '09. New York, New York, USA: ACM Press; 2009, p. 106. http://dx.doi.org/10.1145/1542362.1542388.

[39] Amenta N, Choi S, Kolluri RK. The power crust, unions of balls, and the medial axis transform. Comput Geom 2001;19(2–3):127–53. http://dx.doi.org/10.1016/S0925-7721(01)00017-7.

[40] Miklos B. The scale axis transform (Ph.D. thesis), Zürich: ETH Zürich; 2010.

[41] Hesselink WH, Roerdink J. Euclidean skeletons of digital image and volume data in linear time by the integer medial axis transform. IEEE Trans Pattern Anal Mach Intell 2008;30(12):2204–17. http://dx.doi.org/10.1109/TPAMI.2008.21.

[42] Palágyi K, Kuba A. Directional 3D thinning using 8 subiterations. In: Goos G, Hartmanis J, van Leeuwen J, Bertrand G, Couprie M, Perroton L, editors. Discrete geometry for computer imagery. Lecture notes in computer science, Vol. 1568, Berlin, Heidelberg: Springer Berlin Heidelberg; 1999, p. 325–36. http://dx.doi.org/10.1007/3-540-49126-0{_}25.

[43] van Dortmont MAMM, van de Wetering HMM, Telea AC. Skeletonization and distance transforms of 3D volumes using graphics hardware. In: Hutchison D, Kanade T, Kittler J, Kleinberg JM, Mattern F, Mitchell JC, Naor M, Nierstrasz O, Pandu Rangan C, Steffen B, Sudan M, Terzopoulos D, Tygar D, Vardi MY, Weikum G, Kuba A, Nyúl LG, Palágyi K, editors. Discrete geometry for computer imagery. Lecture notes in computer science, Vol. 4245, Berlin, Heidelberg: Springer Berlin Heidelberg; 2006, p. 617–29. http://dx.doi.org/10.1007/11907350{_}52.

[44] Yan Y, Letscher D, Ju T. Voxel cores. ACM Trans Graph 2018;37(4):1–13. http://dx.doi.org/10.1145/3197517.3201396.

[45] Jalba AC, Kustra J, Telea AC. Surface and curve skeletonization of large 3D models on the GPU. IEEE Trans Pattern Anal Mach Intell 2013;35(6):1495–508. http://dx.doi.org/10.1109/TPAMI.2012.212.

[46] Dey TK, Zhao W. Approximate medial axis as a voronoi subcomplex. In: Seidel H-P, Shapiro V, Lee K, Patrikalakis N, editors. Proceedings of the seventh ACM symposium on solid modeling and applications - SMA '02. New York, New York, USA: ACM Press; 2002, p. 356. http://dx.doi.org/10.1145/566282.566333.

[47] Dey TK, Woo H, Zhao W. Approximate medial axis for CAD models. In: Turkiyyah G, Brunet P, Elber G, Shapiro V, editors. Proceedings of the eighth ACM symposium on solid modeling and applications - SM '03. New York, New York, USA: ACM Press; 2003, p. 280. http://dx.doi.org/10.1145/781606.781652.

[48] Foskey M, Lin MC, Manocha D. Efficient computation of a simplified medial axis. In: Turkiyyah G, Brunet P, Elber G, Shapiro V, editors. Proceedings of the eighth ACM symposium on solid modeling and applications - SM '03. New York, New York, USA: ACM Press; 2003, p. 96. http://dx.doi.org/10.1145/781606.781623.

[49] Chazal F, Lieutier A. The ''λ-medial axis''. Graph Models 2005;67(4):304–31. http://dx.doi.org/10.1016/j.gmod.2005.01.002.

[50] Taha AA, Hanbury A. An efficient algorithm for calculating the exact Hausdorff distance. IEEE Trans Pattern Anal Mach Intell 2015;37(11):2153–63. http://dx.doi.org/10.1109/TPAMI.2015.2408351, URL: http://ieeexplore.ieee.org/document/7053955/.

[51] Bendse MP, Kikuchi N. Generating optimal topologies in structural design using a homogenization method. Comput Methods Appl Mech Engrg 1988;71(2):197–224. http://dx.doi.org/10.1016/0045-7825(88)90086-2, URL: https://www.sciencedirect.com/science/article/pii/0045782588900862.

[52] Van Rossum G. The python library reference, release 3.8.2. Python Software Foundation; 2020.

[53] Harris CR, Millman KJ, van der Walt SJ, Gommers R, Virtanen P, Cournapeau D, Wieser E, Taylor J, Berg S, Smith NJ, Kern R, Picus M, Hoyer S, van Kerkwijk MH, Brett M, Haldane A, del Río JF, Wiebe M, Peterson P, Gérard-Marchant P, Sheppard K, Reddy T, Weckesser W, Abbasi H, Gohlke C, Oliphant TE. Array programming with NumPy. Nature 2020;585(7825):357–62. http://dx.doi.org/10.1038/s41586-020-2649-2.

[54] The pandas development team. Pandas-dev/pandas: Pandas. 2020, http://dx.doi.org/10.5281/zenodo.3509134.

[55] The Trimesh development team. Trimesh [computer software]. 2020, URL: https://github.com/mikedh/trimesh.

[56] Sullivan CB, Kaszynski A. PyVista: 3D plotting and mesh analysis through a streamlined interface for the visualization toolkit (VTK). J Open Source Softw 2019;4(37):1450. http://dx.doi.org/10.21105/joss.01450.

[57] Virtanen P, Gommers R, Oliphant TE, Haberland M, Reddy T, Cournapeau D, Burovski E, Peterson P, Weckesser W, Bright J, van der Walt SJ, Brett M, Wilson J, Millman KJ, Mayorov N, Nelson ARJ, Jones E, Kern R, Larson E, Carey CJ, Polat I, Feng Y, Moore EW, VanderPlas J, Laxalde D, Perktold J, Cimrman R, Henriksen I, Quintero EA, Harris CR, Archibald AM, Ribeiro AH, Pedregosa F, van Mulbregt P, SciPy 10 Contributors. SciPy 1.0: Fundamental algorithms for scientific computing in Python. Nature Methods 2020;17:261–72. http://dx.doi.org/10.1038/s41592-019-0686-2.

[58] Hagberg AA, Schult DA, Swart PJ. Exploring Network Structure, Dynamics, and Function using NetworkX. In: Gaël Varoquaux and Travis Vaught and Jarrod Millman (eds.) Proceedings of the 7th Python in science conference, Pasadena, CA USA, 2008, p. 11–15.

[59] Attene M. A lightweight approach to repairing digitized polygon meshes, 26, (11), 2010, 1393–1406. http://dx.doi.org/10.1007/s00371-010-0416-3, PII: 416.

[60] Musy M, Jacquenot G, Dalmasso G, neoglez, de Bruin R, Pollack A, Claudi F, Badger C, icemtel, Sullivan B, Hrisca D, Volpatto D, Schlömer N, Zhou Z-Q, ilorevilo. Vedo, a python module for scientific analysis and visualization of 3D objects and point clouds. 2021, http://dx.doi.org/10.5281/zenodo.4287635.

[61] Carlier A, Leonard K, Hahmann S, Morin G, Collins M. The 2D shape structure dataset: A user annotated open access database. Comput Graph 2016;58:23–30. http://dx.doi.org/10.1016/j.cag.2016.05.009.

[62] Abadi M, Agarwal A, Barham P, Brevdo E, Chen Z, Citro C, Corrado GS, Davis A, Dean J, Devin M, Ghemawat S, Goodfellow I, Harp A, Irving G, Isard M, Jia Y, Jozefowicz R, Kaiser L, Kudlur M, Levenberg J, Mané D, Monga R, Moore S, Murray D, Olah C, Schuster M, Shlens J, Steiner B, Sutskever I, Talwar K, Tucker P, Vanhoucke V, Vasudevan V, Viégas F, Vinyals O, Warden P, Wattenberg M, Wicke M, Yu Y, Zheng X. TensorFlow: Large-scale machine learning on heterogeneous systems. 2015, URL: https://www.tensorflow.org/, Software available from tensorflow.org.